

## EXPERIMENTAL AND NUMERICAL STUDIES ON PUSH-UP LOAD TESTS FOR SAND PLUGS IN A STEEL PIPE PILE

SURIYAH THONGMUNEE<sup>i)</sup>, TATSUNORI MATSUMOTO<sup>ii)</sup>, SHUN-ICHI KOBAYASHI<sup>iii)</sup>,  
 PASTSAKORN KITTIYODOM<sup>iv)</sup> and KEN KUROSAWA<sup>v)</sup>

### ABSTRACT

This paper focuses on the bearing capacity of soil plugs (internal shaft resistance) through fundamental research on the bearing mechanism of dry silica sand plugs. Push-up load tests on the dry silica sand plugs inside a model pipe pile and DEM simulations were carried out to investigate the plugging behaviour. The influences of the packing state of the soil plugs (the relative density), and the height of the plugs on the bearing capacity were investigated. Prior to the push-up load tests, element tests on the silica sand and DEM analyses were performed to characterise the silica sand and to determine suitable DEM analysis parameters. The experimental and DEM results clearly show that the push-up force increases significantly with the increase in the aspect ratio of the soil plug,  $H/D$ , and with the relative density of the soil plug. The DEM analyses show a good agreement with the experimental results when the push-up force is small. Furthermore, the DEM results reveal that only the density of the soil plug in the lower portion, adjacent to the pile tip, increases gradually with the increase in the push-up displacement as well as the increase in  $H/D$ . Hence, it is the lower portion of the soil plug that mainly controls the capacity of the soil plug.

**Key words:** discrete element method, dry sand, laboratory soil test, open-ended steel pipe pile, plugging, push-up load test (IGC: E4/E13/E14)

### INTRODUCTION

Open-ended pipe piles are widely used for foundations in many countries. During the driving process, a soil column is created inside the pipe pile which is known as a soil plug. Depending on the relative motion between the pile and the soil plug, the pile is said to be plugged, partially plugged or unplugged, as has been stated by Matsumoto et al. (2004) and so on. If the pipe pile is completely plugged, the soil plug will move together with the pipe pile. On the other hand, if the pipe pile is completely unplugged, the soil plug will not move with the pile. And, if the pipe pile is partially plugged, the soil plug will move relative to the pile, so that the height of the soil plug inside the pipe pile will be some fraction of the total embedded pile length. However, during the driving process of an open-ended pipe pile, it is difficult to obtain either fully plugged or completely unplugged conditions. Figure 1 shows the bearing components of an open-ended pipe pile. The bearing capacity of an open-ended pipe pile consists of three components, namely, the outer shaft capacity,  $Q_{out}$ , the toe capacity of the annular pile base,  $Q_{toe}$ , and the soil plug capacity,  $Q_{plug}$  (Fig. 1(a)). From the force

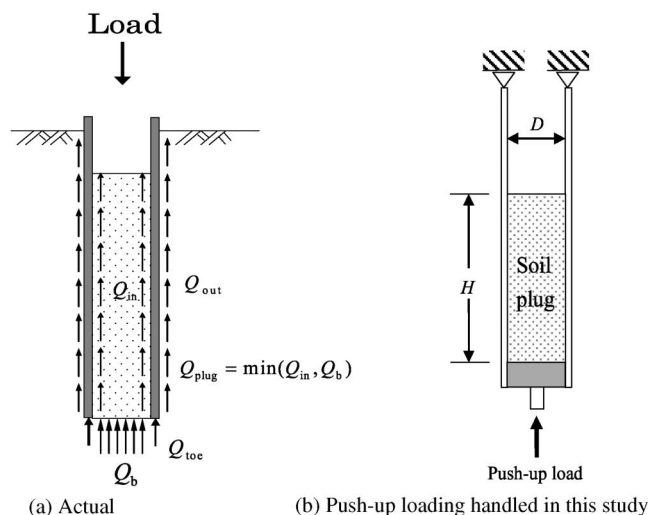


Fig. 1. Bearing mechanism of open-ended pipe pile

equilibrium,  $Q_{plug}$  is the smaller value of the potential inner shaft capacity,  $Q_{in}$ , or the bearing capacity of the soil beneath the plug base,  $Q_b$ .

<sup>i)</sup> Ph. D candidate, Graduate School of Natural Science and Technology, Department of Civil Engineering, Kanazawa University, Kanazawa, Japan (thongmunee@hotmail.com).

<sup>ii)</sup> Professor, ditto (matsumot@t.kanazawa-u.ac.jp).

<sup>iii)</sup> Associate Professor, ditto (koba@t.kanazawa-u.ac.jp).

<sup>iv)</sup> Senior Engineer, Geotechnical and Foundation Engineering Co., Ltd., Thailand.

<sup>v)</sup> Engineer, Takasaki City, Takasaki, Japan (former student of Kanazawa University).

The manuscript for this paper was received for review on April 27, 2010; approved on June 8, 2011.

Written discussions on this paper should be submitted before May 1, 2012 to the Japanese Geotechnical Society, 4-38-2, Sengoku, Bunkyo-ku, Tokyo 112-0011, Japan. Upon request the closing date may be extended one month.

Considering the above-mentioned bearing mechanism of the pipe pile, an understanding of the plugging mechanism is a key factor in the estimation of the total capacity of an open-ended pipe pile. Hence, as the first step, this study focuses on soil plug behaviour alone in order to understand the bearing mechanism of an open-ended pipe pile. In this study, to investigate the plugging behaviour, push-up load tests for sand plugs inside an open-ended steel pipe pile, as shown in Fig. 1(b), are carried out, and DEM analyses are conducted to gain more insight into the plugging mechanism.

## REVIEW OF RELATED RESEARCH

Theoretical, experimental and numerical studies on plugging or the push-up loading of soil plugs have been done by many researchers, as Matsumoto et al. (2004) summarised. The related research works on open-ended pipe piles in Japan and other countries are briefly reviewed below.

Yamahara (1964a) derived theoretical equations for estimating the vertical pressure of uniform soil plugs and the inner shaft capacity of sand and clay. In his theory, the force equilibrium of a thin soil plug element is employed and the soil plug is assumed to be a rigid body.

Yamahara (1964b) derived a solution for the distribution of axial forces along an open-ended pipe pile from the equilibrium of applied force at the pile head and the inner shaft resistance. Although the deformability of the soil and the pile is not taken into account in the solution, it was demonstrated from field load tests on an open-ended steel pile that the measured distribution of axial forces was predicted well by the theoretical solution. Yamahara (1964b) also conducted direct shear tests on steel and soil to estimate and compare the coefficients of friction for the pile and the soil,  $\mu$ , and special oedometer tests to estimate the coefficients of lateral pressure,  $\nu$ . In the specially designed oedometer tests, both the lateral pressure at rest and the vertical pressure were measured.

Kishida and Isemoto (1977) carried out push-up load tests for dry dense sand plugs employing pipe piles with five different inner pile diameters,  $D_i$  (300 mm to 1000 mm). The tests were carried out for 16 cases in which the ratio of the height of the dry sand plug to the inner pile diameter,  $H/D_i$ , were varied. FEM analyses of the tests were also carried out in which the slippage between the soil plug and the inner shaft surface of the pipe pile was taken into account. The results of the push-up load tests and the analyses show that the area around the bottom of the soil plug is subjected to a great amount of compaction, and that the push-up load is mostly supported by the friction resistance along that part of the soil plug. The ultimate push-up load increases with the increase in the aspect ratio of the soil plug,  $H/D_i$ .

Kanno et al. (1978) performed a series of push-up load tests for dry sand plugs inside open-ended steel pipe piles. Four different inner diameters of open-ended steel pipe piles were employed. The ratio of the height of the soil plug to the inner pile diameter,  $H/D_i$ , varied from 2 to 5

for each pipe pile. It was found from the test results that the maximum push-up stress is related to the aspect ratio of the soil plug,  $H/D_i$ , for a given inner pile diameter, and that the maximum push-up stress tends to increase with the increase in inner pile diameter for a given value of  $H/D_i$ .

Paikowski and Whitman (1990) examined the effects of plugging on pile performance and design in reference to the ultimate static capacity, time-dependent pile capacity and dynamic behaviour. Plugging was found to have a great influence on the marked contribution of the capacity of piles driven in sand, the delay in capacity gain with time for piles driven in clay and changes in the behaviour of piles during installation.

Leong and Randolph (1991) carried out finite element analyses of the soil plug response under drained, undrained and partially drained conditions. The soil plugs were modelled as elastic, elastic-perfectly-plastic (Mohr-Coulomb) and elasto-plastic (modified Cam clay). Elastic-perfectly-plastic joint elements were employed to model the soil-pile interface. No softening effect of the interface was considered. The model soil plug tests (Randolph et al., 1992) were compared with the finite element analyses. Parametric studies were also performed on the effect of soil permeability on soil plug capacity. They suggested that the soil plug capacity, under partially drained conditions, is sensitive to the interface friction angle, the loading rate, the consolidation characteristics of the soil and the aspect ratio of the soil plug.

Randolph et al. (1991) and Randolph et al. (1992) presented a simple one-dimensional analysis of a soil plug under partially undrained conditions to estimate the bearing capacity of a pipe pile under faster rates of loading relevant to an offshore environment where the increase in effective stress within the soil plug is limited and the plug capacity is significantly lower. Based on the proposed method, a computer program entitled SPA (Soil Plug Analysis) was developed.

Byrne (1995) conducted a number of field tests on small pipe piles driven into dense sand under a variety of pile tip conditions, varying from close-ended to open-ended, and employing three different types of internal sleeves. The sleeves led to improved drivability, with more soil entering the piles to form soil plugs. However, it was also found that the end bearing capacity of the piles decreased linearly with the increase in the plugging ratio. The measured pile capacity was significantly higher than that estimated using the design code.

Hight et al. (1996) examined the effect of pile diameter on the end bearing capacity of open-ended pipe piles driven in sand by conducting laboratory tests (push-up load tests), finite element analyses and a data base study of load tests on open-ended piles of various diameters driven in sand. From the results of the push-up load tests for sand plugs, they pointed out that there exists a critical height for the plug,  $h_{crit}$ . When the sand column height,  $h$ , is less than  $h_{crit}$ , the whole sand plug is displaced, the lock-up of the sand plug does not occur and residual push-up force is obtained in all packing states. In contrast, when  $h$

is more than  $h_{crit}$ , the sand plug can lock-up and develop high resistance. The value of  $h_{crit}$  decreases as the density of the soil plug increases and as the pile diameter decreases. The FEM results confirm the effect of pile diameter in terms of the decreasing influence of a dilatant annular zone at the pile wall as the pile diameter increases. Based on the data base study, the lock-up in a medium dense sand column does not occur in piles having diameters greater than 700 mm.

de Nicola and Randolph (1997) conducted a series of model pile tests using the geotechnical centrifuge to study the plugging behaviour of piles in sand. Open-ended pipe piles were driven and jacked by a miniature pile driving actuator into silica flour of various densities. The progression of the soil plug was measured during installation and static loading. It was found from the test results that the plug length increased with the increase in relative density during driving and decreased with the increase in relative density during jacking. During installation, the jacked piles exhibited a greater tendency to plug than the driven piles.

Liyanapathirana et al. (1998, 2000, 2001) carried out a series of finite element analyses of open-ended pipe piles as follows.

Liyanapathirana et al. (1998) investigated the plugging mechanism of infinitely-long open-ended piles using a numerical simulation of the wave propagation inside soil plugs and piles. The results show that the key parameters for the plugging mechanism are the pile radius, the shape of the impact load, the shear wave velocity of the soil inside the pile and the friction at the pile-soil interface. These parameters can be used to assess whether the pile plugs or not during driving.

Liyanapathirana et al. (2000) presented a new finite element technique to analyse the driving response of open-ended piles subjected to multiple hammer blows. It was found that the increment filling ratio (IFR) at the pile tip is higher than that observed at the top of the soil plug at the end of the first blow. After several blows, the IFR becomes uniform along the length of the soil plug. The results suggest that the soil plug is compressed at the beginning and reaches the residual state after several blows. In addition, a difference in the soil flow around the pile was observed in the analyses, when the pile was unplugged or partially plugged. In the latter case, the soil below the pile tip moved in the radially outward direction. This supports the results whereby the yielded zone around the pile tip in a partially plugged pile is usually three times the size of that in an unplugged pile.

Liyanapathirana et al. (2001) carried out a numerical study on the thin-walled open-ended piles during the driving process to examine the stress wave propagation in the vicinity of the pile toe. The results indicate that the shear stress had the maximum magnitude above the bottom of the soil plug. Beneath the bottom of the soil plug, the vertical stress wave had the highest magnitude. Moreover, the maximum vertical stress at the bottom of the soil plug appears after the vertical stress wave interacts with the shear stress wave in the radial direction. They suggested

that the interaction between the waves travelling in radial and vertical directions at the bottom of the soil plug was considerable.

Paik and Salgado (2003) focused on the effect of the increment filling ratio (IFR) on the pile load capacity. Model pile load tests were conducted on instrumented open-ended piles using a calibration chamber. The results indicate that the IFR plays an important role in the base and shaft resistances of open-ended piles. The base and shaft resistances increase with the increase in the IFR. The results also indicate that the IFR increases with the increase in relative density and horizontal stress, but that it is independent of the vertical stress. Moreover, the IFR decreases linearly with the ratio of soil plug length to pile penetration depth (PLR) and can be predicted from the PLR.

Paik et al. (2003) performed field load tests on open-ended and closed-ended pipe piles driven into sand to investigate the effect of the soil plug on the static and dynamic responses of the open-ended pipe pile. And, the sharing of load capacity of both the piles was investigated. It was observed that the capacity of the open-ended pipe pile was lower than that of the closed-ended pipe pile at the same depth, but that the difference was predominant at the early stages of driving when the soil plug was not well developed. The results also show that the unit base and the shaft resistances of the open-ended pipe pile were lower than those of the closed-ended pile. The unit base and the shaft resistances of the open-ended pipe pile were 30% and 58% of those of the closed-ended pile at the same settlement of 10% of pile diameter. For the open-ended pipe pile, the average shear stress between the soil plug and the inner pile surface was 36% higher than the outer shaft resistance.

Gavin and Lehane (2003) conducted a series of model pile load tests in a large testing chamber in order to investigate the important factors influencing the shaft capacity of open-ended piles in sand. The results indicate that local maximum shear stress, which can develop on the inner shaft of a pipe pile, depends on the incremental filling ratio (IFR) during installation, the aspect ratio of the soil plug ( $h/D$ ) and the  $q_c$  value in cone penetration tests (CPT). In addition, the average end bearing stress at the base of a pipe pile during driving can be expressed as a function of IFR,  $h/D$  and the  $q_c$  value as well.

Kitiyodom et al. (2004) carried out a series of model tests in dry silica sand in a 1 g field, in order to clarify the effect of the soil plug on the bearing capacity of driven open-ended pipe piles. With the aim to increase the bearing capacity of the driven pipe piles, due to the increase in the soil plugging effect, different pile conditions, such as a hollow pile, the attachment of a cross-shaped steel brace and the increase in the coefficient of friction at the inner surface, were employed. Each model pipe pile was driven into a model ground by a falling hammer until the pile toe reached a prescribed depth. Then, static axial compression pile load tests were carried out. Thereafter, the model pile was re-driven into the ground. Finally, static axial tensile pile load tests were conducted. The height of

the soil plug inside the pile was measured throughout the tests. It was found that only partial plugging of the open-ended pipe piles occurred during the driving process. The effect of the soil plugging increased along with the increase in the friction coefficient between the soil plug and the pipe pile and with the increase in the inner shaft interface area.

Kitiyodom et al. (2004) also carried out an analytical study on the soil plugging of an open-ended steel pipe pile in sand using a computer program entitled KWAVE (Matsumoto and Takei, 1991). The soil plug was modelled as a series of masses and springs with frictional forces between the soil nodes and pile nodes. In the pile driving analysis, stress waves propagating up and down the soil plug were calculated based on Smith's model, whereas the characteristic solutions of the wave equation were adopted to calculate the wave propagation in the pile. The results show that the pile/soil modelling used in the study can simulate the behaviour of the pile, the soil and the soil plug during static loading and driving, if the soil parameters are selected appropriately.

## OBJECTIVE OF THIS PAPER

As mentioned in the previous section, the plugging or the push-up loading of soil plugs has been investigated by many approaches. The results clearly show that the soil plug capacity of an open-ended pipe pile mainly depends on the pile diameter, the height of the soil plug, the soil-pile interface friction coefficient and the relative density of the soil plug. Furthermore, the area around the bottom of soil plug contributes greatly to the soil plug capacity.

However, it is questionable whether the above-mentioned results are sufficient for understanding the plugging mechanism and the formation of soil plugs in order to evaluate the inner shaft resistance quantitatively. In other words, neither volume changes of the soil plug due to compression stress or dilatancy during pile installation nor the behaviour of the soil surrounding or inside the pipe pile subjected to large deformations and failures is fully understood.

In this paper, experimental and numerical studies on the push-up loading of dry silica sand plugs within a steel pipe pile were carried out to investigate the plugging mechanism and the formation of soil plugs. Focus is placed on the influence of the packing state (relative density) and the height of the soil plugs on the push-up force. The Discrete Element Method (DEM) was employed to simulate the experiments to gain more insight into the plugging behaviour. DEM is a numerical technique used extensively to model the mechanical behaviour of granular assemblies (Cundall and Strack, 1979).

Prior to the push-up load tests and its DEM analyses, laboratory tests on silica sand were carried out to characterise the silica sand. The laboratory tests included element tests and shear tests between the silica sand and the model pile. Then, DEM simulations of the element tests, including maximum and minimum dry density tests, one-

dimensional compression tests and direct shear tests, were carried out to determine the suitable input analysis parameters to be used in the DEM analyses of the push-up load tests. The DEM simulations of the laboratory tests and the push-up load tests were carried out without giving consideration to particle crushing.

Moreover, the test results of the push-up load tests on the dry silica sand plugs are compared with the results obtained from Yamahara's theoretical equation. A discussion on the influence of the dilatancy behaviour of the soil plug on its capacity is made.

## INVESTIGATION OF SILICA SAND

The laboratory tests on the silica sand consisted of element tests on the silica sand, and shear tests between the silica sand and the inner shaft surface of the model pile.

Element tests, such as particle density tests, maximum and minimum dry density tests, one-dimensional compression tests and direct shear tests, were firstly carried out. Then, the shear tests were performed to obtain the interface friction coefficient between the silica sand and the inner shaft surface of the model pile for use in the DEM simulations of the push-up load tests.

### *Element Tests on Silica Sand*

Particle density tests and maximum and minimum dry density tests were carried out on the silica sand following the standard method by the Japanese Geotechnical Society (1992). The results are summarised in Table 1. The silica sand has relatively uniform particle sizes.

One-dimensional compression tests on the dry silica sand were performed using a cylindrical box with an inner diameter of 60 mm and a height of 40 mm. The compression tests were conducted for specimens in three different packing states, namely, the loose state ( $D_r = 50$  to 60%), the medium state ( $D_r = 70$  to 80%) and the dense state ( $D_r \geq 90\%$ ).

Direct shear tests on the silica sand were carried out us-

**Table 1. Physical properties of dry silica sand**

Property	Value
Density of soil particle, $\rho_s$	2.68 t/m <sup>3</sup>
Maximum dry density, $\rho_{d \max}$	1.69 t/m <sup>3</sup>
Minimum dry density, $\rho_{d \min}$	1.39 t/m <sup>3</sup>
Maximum void ratio, $e_{\max}$	0.927
Minimum void ratio, $e_{\min}$	0.583
Mean grain size, $D_{50}$	0.126 mm
Coefficient of uniformity, $U_c$	2.27

**Table 2. Strength parameters of dry silica sand**

Packing state of sand	$c'$ (kPa)	$\phi'$ (deg.)
Loose (at peak)	17.44	33.5
Medium (at peak)	11.52	35.4
Dense (at peak)	9.03	36.0
Residual state (average)	9.83	32.0

ing a shear box with an inner diameter of 60 mm and a height of 35 mm. The strength parameters in each packing state of the silica sand obtained from the direct shear tests are summarised in Table 2.

The detailed results of the maximum and minimum density tests, the compression tests and the direct shear tests will be shown later in this paper for a comparison with the DEM simulation results.

*Shear Test between the Silica Sand and the Model Pile*

Shear tests on the silica sand and the inner shaft surface of the model pile were performed in order to estimate the intrinsic friction coefficient between the sand particles and the inner pile surface to be used in the DEM analysis.

In the DEM simulations of the push-up load tests on the silica sand plug within the pile, the sand plug is modelled as an assembly of rigid particles and the pile is modelled by rigid wall elements. The intrinsic friction coefficient, not internal friction coefficient, between the wall and the particle without rotation is required in the DEM analyses to model the interface behaviour.

A steel pipe pile was used for the model pile in this study. The properties of the model pipe pile are summarised in Table 3. Figure 2 and Photo 1 show the test set-up. A plastic bag with sand particles on its surface was placed inside the model pipe pile. The silica sand particles

were glued to the surface of the plastic bag, as shown in Photo 2, to avoid the rotation of the sand particles during shearing. The density of the silica sand on the plastic bag had no influence on the intrinsic friction coefficient. Lead balls placed within the plastic bag were used to control the normal force,  $N$ , between the sand particles and the inner surface of the pile. Normal force,  $N$ , was set at 9.8, 19.6 and 39.2 N. The plastic bag placed inside the model pile was pulled using a winch. Throughout the tests, the friction force,  $F_{\text{fric}}$ , and the horizontal displacement were measured using a load cell and a displacement meter, respectively. The intrinsic friction coefficient,  $\mu$ , was estimated using the general formula ( $\mu = F_{\text{fric}}/N$ ). For accuracy, four shear tests were conducted at each normal force.

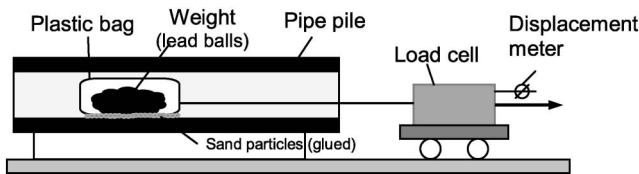
Figure 3(a) shows an example of the results of the shear tests in the case of  $N=9.8$  N. The results from the four tests were very similar and the friction coefficient,  $\mu$ , was obtained as about 0.5. Similar values were also obtained for other normal forces.

Figure 3(b) shows the test results of shear tests between the pile and the silica sand allowing sand particle rotation. The average friction coefficient was about 0.22 (44% of  $\mu$ ). It should be noted that the rotation of the particles had a significant influence on the interface friction coefficient between the sand particles and the pile shaft surface.

The value of the sand-pile friction coefficient,  $\mu$ , without particle rotation ( $\mu=0.5$ ) will be used in the DEM analyses of the push-up load tests on the sand plug as the particle-wall intrinsic friction coefficient.

**Table 3. Properties of model pipe pile**

Property	Value
Young's modulus	201 GPa
Length	1100 m
Inner diameter	93.2 mm
Outer diameter	101.4 mm



**Fig. 2. Illustration of device for direct shear tests between sand and inner surface of pipe pile (not to scale)**

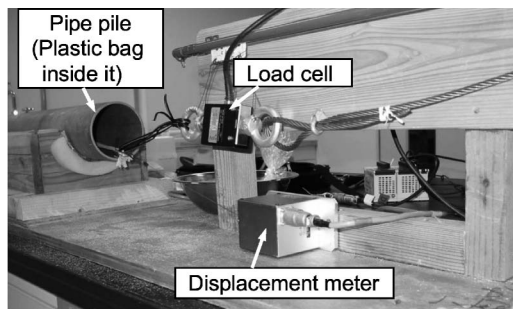


**Photo 1. Device for direct shear tests between sand and inner surface of pipe pile**

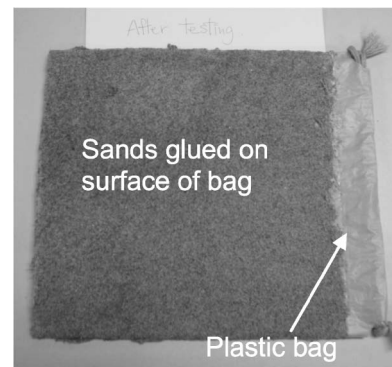


**Photo 2. Plastic bag coated by silica sand for direct shear tests between sand and inner shaft surface of pipe pile**

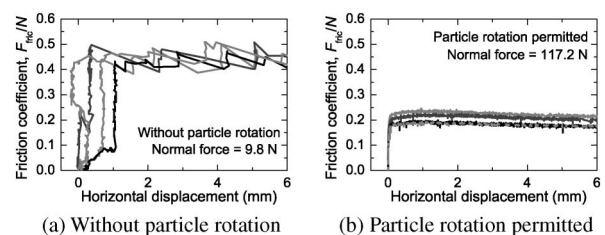


**Fig. 3. Example of results of direct shear tests between sand and inner surface of pipe pile**

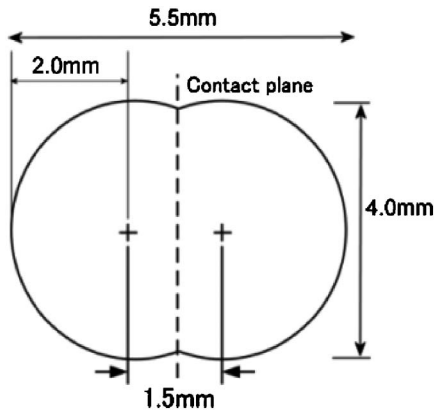


Fig. 4. Peanut-shaped clump used in DEM analyses

### DETERMINATION OF ANALYSIS PARAMETERS

The DEM code, called *PFC3D* (Itasca, 2003), was employed in this study. The silica sand particles were modelled using a rigid peanut-shaped clump. Hence, the deformation and the crushing of the clump particles were not taken into account. The clump is composed of two rigid identical spheres that partially overlap to form non-spherical particles (e.g., Katzenbach and Schmitt, 2004; Yan, 2009; Thongmunee et al., 2010).

It is desirable to use the same particle size as real sand in DEM. However, such modeling is difficult in practice, from the viewpoint of calculation capacity and calculation time. In centrifuge tests carried out by Ovesen (1979), no scale effect was observed for the model footings that had ratios of footing diameter to soil particle size ranging from 30 to 180. The inner diameter of the model pile (diameter of sand plug) was 93.2 mm. According to the above observations in the centrifuge tests, the particle size to be used in DEM should be less than 3 mm. However, the use of clumps consisting of two spheres with a diameter of 3 mm took a very long calculation time. Hence, peanut-shaped clumps with a diameter of 4 mm, as shown in Fig. 4, were used. Although the authors are aware that particle size has an influence on dilatancy behaviour in DEM results, there was no other choice for reducing the calculation time.

Numerical studies on direct shear tests using 3D-DEM have been carried out by, for example, O'Sullivan et al. (2004) and Härtl and Ooi (2008). Following their research works, matching analyses of the direct shear tests were conducted in this study to determine suitable input analysis parameters for DEM analyses.

Prior to DEM simulations of the direct shear tests on silica sand, DEM analyses of the laboratory tests, including the maximum and minimum density tests and one-dimensional compression tests, were carried out. Note here again that the DEM simulations of the laboratory tests were carried out without giving consideration to particle crushing.

#### Simulations of Maximum and Minimum Density Tests

Figure 5 shows the analytical models for the maximum

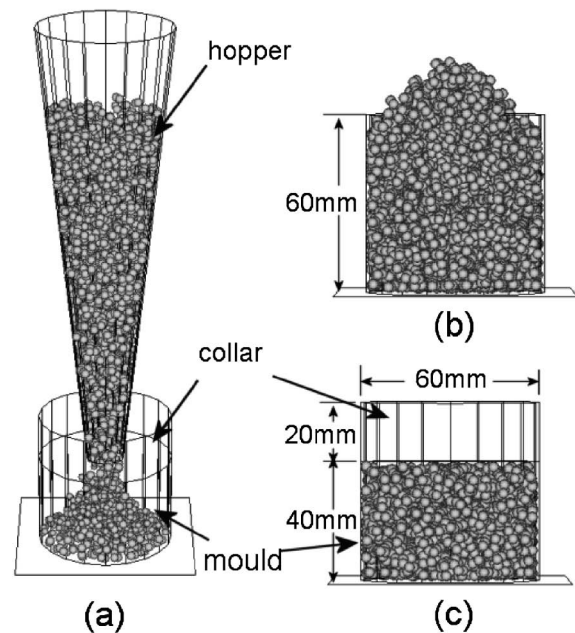


Fig. 5. Analysis models used for minimum density and maximum density tests

Table 4. Analysis parameters and properties of clump

Property	Value
Particle size (Long axis)	5.5 mm
(Short axis)	4.0 mm
Density of clump particles, $\rho_s$	2.73 t/m <sup>3</sup>
Friction coefficient between clumps, $\phi_\mu$	0.7
Surface friction coefficient between clump and wall	0.5
Normal and tangential spring stiffness between clumps	10 <sup>6</sup> N/m
Normal and tangential spring stiffness between clump and wall	10 <sup>6</sup> N/m

and minimum density tests on the silica sand. The hopper, mould and collar were modelled by 'wall elements'. The input analysis parameters for both tests are summarised in Table 4. The surface friction coefficient between the clump and the wall was set at 0 and then disregarded.

For the minimum density tests, rigid clumps were generated inside the hopper (Fig. 5(a)). Then, a self-weight analysis was conducted. After that, the hopper was pulled-up at a speed of 5 mm/s. After the clump particles had dropped into the mould with the collar (Fig. 5(b)), the clump particles in the collar were eliminated and the maximum void ratio,  $e_{\max}$ , of the sand in the mould was calculated (Fig. 5(c)). The results of the DEM analyses of the minimum density tests show that the mean values for the maximum void ratio and the minimum dry density were 0.958 and 1.397 t/m<sup>3</sup>, respectively.

The maximum density tests were started from the state shown in Fig. 5(b). Sinusoidal horizontal displacement, having a frequency of 5 Hz and an amplitude of 5 mm, was applied to the mould to model the impact on the mould. One thousand shaking cycles were applied to the mould. The shaking direction was changed by 36 degrees

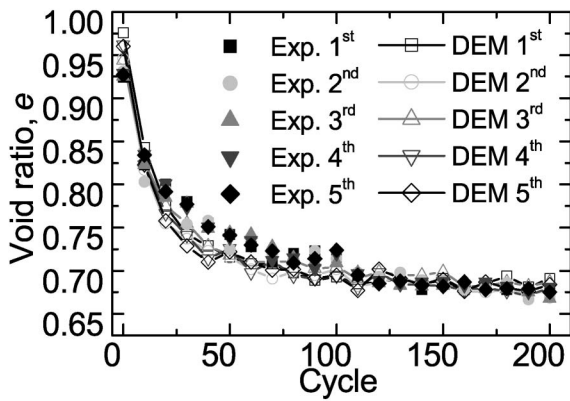


Fig. 6. Calculated and experimental results of maximum density tests up to 200 shaking cycles

Table 5. Comparison between measured and calculated results

Property	Measured	Calculated
Maximum dry density, $\rho_{d \max}$ ( $t/m^3$ )	1.690	1.631
Minimum void ratio, $e_{\min}$	0.583	0.676
Minimum dry density, $\rho_{d \min}$ ( $t/m^3$ )	1.389	1.397
Maximum void ratio, $e_{\max}$	0.920	0.958

every 10 cycles of shaking in the analysis to simulate the testing procedure used. Five analyses were carried out under the same initial conditions before the shaking. Figure 6 shows the changes in void ratio calculated in DEM compared with the laboratory test results. The changes in void ratio versus the number of shaking cycles up to 200 shaking cycles are depicted, although 1000 shaking cycles were applied. The DEM results show a good agreement with the laboratory test results. The void ratio rapidly decreased with the increase in shaking cycles up to 100 cycles and then almost levelled off for further shaking cycles.

Table 5 summarises the DEM results of the minimum and maximum density tests compared with the experimental results. The DEM analyses were able to simulate the experimental results well.

#### Simulations of One-dimensional Compression Tests

DEM simulations of the one-dimensional compression tests on the silica sand were carried out using the analysis parameters listed in Table 4. The surface friction coefficient between the clump and the wall was set at 0 and then disregarded. The DEM simulations were carried out for three different packing states, including the loose state ( $D_r = 50$  to 60%), the medium state ( $D_r = 70$  to 80%) and the dense state ( $D_r \geq 90\%$ ). The initial void ratios prior to compression were set at 0.808, 0.746 and 0.690, respectively.

In the process of the DEM analysis, the one-dimensional compression test box was modelled using wall elements (similar to Fig. 5(c)). The clump particles were generated inside the model compression box. Then, the loading plate was modelled using the wall element at the

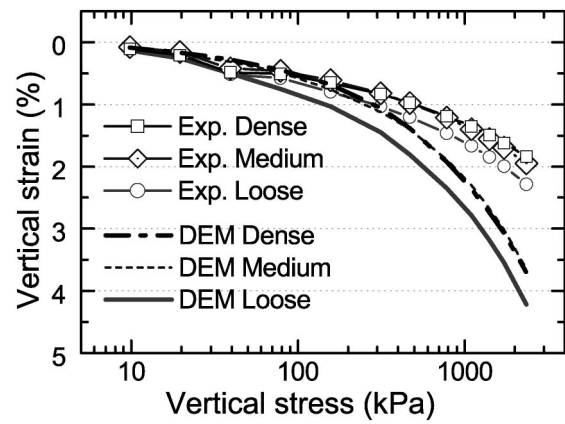


Fig. 7. Calculated and experimental results of one-dimensional compression tests in medium state

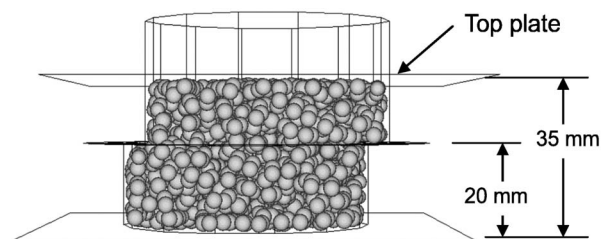


Fig. 8. Analysis model of direct shear tests

top of the specimen. Prior to compression, a self-weight analysis was conducted. Thereafter, a total of eight loading steps, 9.8 to 1254.4 kPa, were applied to the top of the specimen through the wall element.

Figure 7 shows a comparison of the numerical and the experimental results. The DEM analyses simulated the experimental results of the medium and the dense packing states well until a vertical stress of 200 kPa. After the vertical stress of 200 kPa, the DEM analyses overestimated the vertical strain in comparison to the experiments. Similarly, the DEM analysis of the loose state overestimated the vertical strain for vertical stress levels greater than 50 kPa.

Although DEM remarkably overestimated the experimental results, the DEM analyses succeeded in qualitatively simulating the influence of the initial packing state on the compressibility.

#### Simulations of Direct Shear Tests

DEM simulations of direct shear tests on the silica sand in the loose, the medium and the dense states were carried out for a vertical stress of 78.4 kPa using the analysis parameters listed in Table 4. The void ratios, prior to applying the vertical stress, were set at 0.808, 0.746 and 0.689 for the loose, the medium and the dense states, respectively. The friction between the clumps and the side-walls of model box was set at 0 and then disregarded (O'Sullivan et al., 2004; Thongmune et al., 2010). Figure 8 shows the analysis model for the direct shear tests.

In the process of the DEM analysis, the clump particles were generated inside the shear box according to O’Sullivan et al. (2004). The number of clump particles generated in the DEM analyses varied from 1050 to 1200 depending on the packing state of the specimen. Then, a self-weight analysis was conducted. The weight of the loading piston used in the experiments was disregarded, because Härtl and Ooi (2008) suggested that the weight of the test solid on the top of the soil specimen can be ignored for normal stress levels greater than 5 kPa.

Thereafter, normal stress was applied to the top plate. After the completion of the vertical loading stage, horizontal displacement was applied to the upper part of the shear box with a displacement rate of 0.4 mm/min.

Figure 9 shows a comparison of the numerical and the experimental results for different packing states. In the experiments, softening behaviour did not occur in the loose state, while softening behaviour was clearly observed in the medium and the dense states. The DEM analyses were able to simulate these behaviours well and predict the measured strengths well.

As for the dilatancy behaviour (vertical strain), the DEM analyses matched the experimental results for the initial loading stages, i.e., up to shear displacements of 3.5, 2.0 and 1.0 mm in the loose, medium and dense states, respectively. After exceeding these shear displacements, the DEM analyses overestimated the dilatancy behaviour. This tendency became remarkable as the packing state became denser. This discrepancy may be attributed to the fact that the clumps used in the DEM analyses were larger than actual sand particles. The performance of the DEM simulations would be improved, if

smaller particle sizes were used.

Although DEM did not simulate the dilatancy behaviour of the silica sand quantitatively, it was able to qualitatively simulate the influence of the packing state on the dilatancy behaviour. Therefore, the input analysis parameters listed in Table 4 will be used in the DEM analyses of the push-up load tests of sand plugs.

**PUSH-UP LOAD TESTS-EXPERIMENT AND DEM ANALYSIS**

*Experimental Study*

(a) Test Equipment and Arrangement

The push-up load tests on the dry silica sand plugs in the loose, the medium and the dense states were carried out with various aspect ratios. The aspect ratio of the height of the sand plug to the inner pile diameter,  $H/D$ , was varied from 3 to 5, in each packing state. Figure 10 shows an illustration and a photo of the push-up load test device. The test device consists of an oil jack, a load cell, a dial gauge, a rigid loading plate and a model pipe pile.

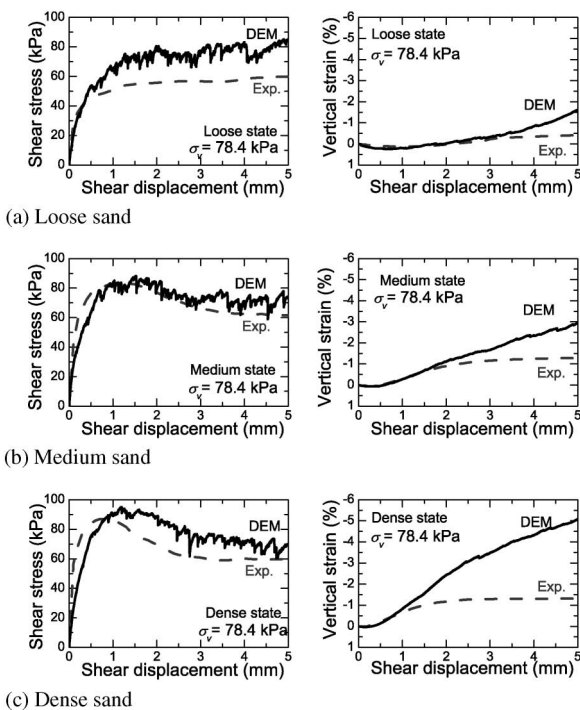
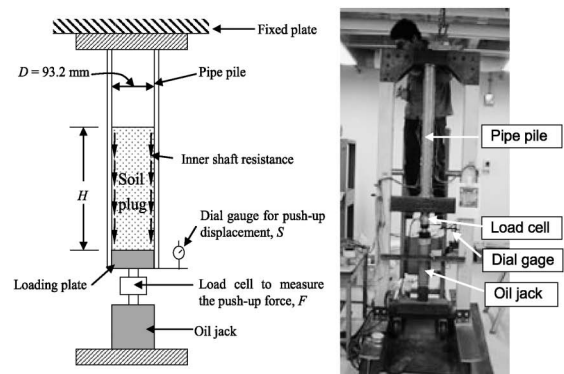


**Fig. 9. Calculated and experimental results of direct shear tests with different initial void ratios**



(a) Illustration of push-up load test (b) Device for push-up load tests

**Fig. 10. Push-up load test device**

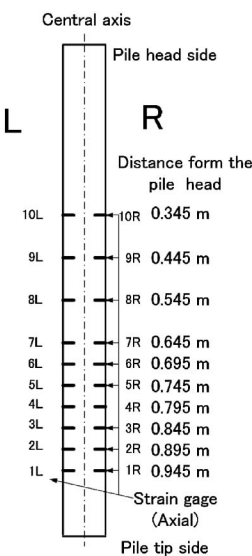


**Fig. 11. Schematic illustration of strain gage arrangement**

The properties of the model pipe pile have been indicated in Table 3.

Figure 11 shows the arrangement of the strain gauges set on the outer surface of the model pile. The model pipe pile was equipped with a total of 20 strain gauges on the left and right sides to measure the axial strains down the pile. The location of each strain gauge is defined by the distance from the pile head. The intervals of strain gauges Nos. 1 to 7 and Nos. 7 to 10 were set at 0.05 m and 0.10 m, respectively.

The axial forces along the pile were calculated directly using the measured axial strain of the model pile assuming that the influence of the radial forces acting on the inner pile shaft on the axial strains was negligible. That is, the axial forces of the pile were calculated as the measured axial strain multiplied by Young’s modulus and the cross-sectional area of the pile. Meanwhile, the shear force between two levels of strain gauges is calculated as the difference in the axial forces at the two levels.

(b) Test Set-up

Firstly, the model pipe pile with the rigid loading plate inside its bottom was set up. The load cell was placed between the oil jack and the loading plate to measure the push-up force,  $F$ . Then, silica sand was poured into the pipe pile from the pipe head by layer. In order to control the specified initial conditions of the sand plug, such as the packing state and the aspect ratio of the sand plug,  $H/D$ , the pile was hit lightly with a rubber hammer. Finally, the dial gauge was installed at the bottom plate to measure the push-up displacement,  $S$ . The push-up force was applied using the oil jack. The push-up displacement rate was maintained at 0.1 to 0.3 mm/s.

(c) Test Results and Discussion

The initial properties of the sand plug in each push-up load test in the loose, the medium and the dense states are summarised in Table 6. Push-up loading was terminated when the push-up force reached 200 kN, which was the

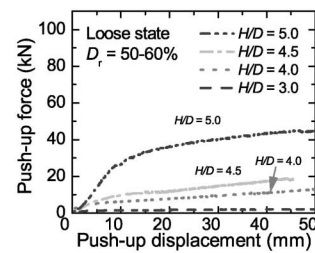
maximum loading capacity of the loading device, or when the push-up displacement reached 50 mm, which was about 50% of the inner pile diameter. Table 7 summarises the measured maximum push-up force in each test.

Figure 12 shows the relationship between the push-up displacement and the push-up force in each packing state. The results indicated that the push-up force significantly increases with the increase in the aspect ratio,  $H/D$ , as well as in the initial packing state of the soil plug. The push-up force continued to increase with the increase in the push-up displacement without showing softening behaviour in any of the cases.

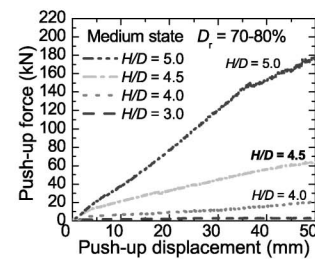
It should be noted that there are slight variations in the soil plug densities, i.e., those of the loose, medium and dense sand plugs were 1.54 t/m<sup>3</sup>, 1.60 t/m<sup>3</sup> and 1.67 t/m<sup>3</sup>, respectively. Accordingly, it is difficult to explain the

Table 7. Measured values of maximum push-up force

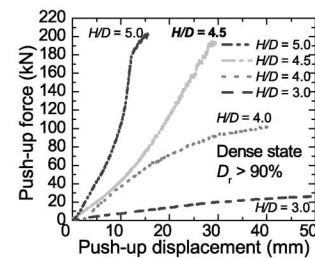
$H/D$	Maximum push-up force (kN)		
	Loose	Medium	Dense
3.0	2.5	4.8	27.5
4.0	14.3	51.9	102.5
4.5	18.7	91.6	197.4
5.0	50.3	199.6	202.8



(a) Loose state



(b) Medium state



(c) Dense state

Table 6. Initial properties of sand plug in push-up tests

a) Loose state

$H/D$	3.0	4.0	4.5	5.0
Relative density, $D_r$ (%)	52	55	55	53
Void ratio, $e$	0.750	0.743	0.739	0.749
Dry density, $\rho_d$ (t/m <sup>3</sup> )	1.53	1.54	1.54	1.53

b) Medium state

$H/D$	3.0	4.0	4.5	5.0
Relative density, $D_r$ (%)	77	72	74	72
Void ratio, $e$	0.663	0.681	0.674	0.683
Dry density, $\rho_d$ (t/m <sup>3</sup> )	1.61	1.59	1.60	1.59

c) Dense state

$H/D$	3.0	4.0	4.5	5.0
Relative density, $D_r$ (%)	98	98	92	93
Void ratio, $e$	0.601	0.601	0.610	0.607
Dry density, $\rho_d$ (t/m <sup>3</sup> )	1.67	1.67	1.67	1.67

Fig. 12. Relationship between push-up displacement and push-up force

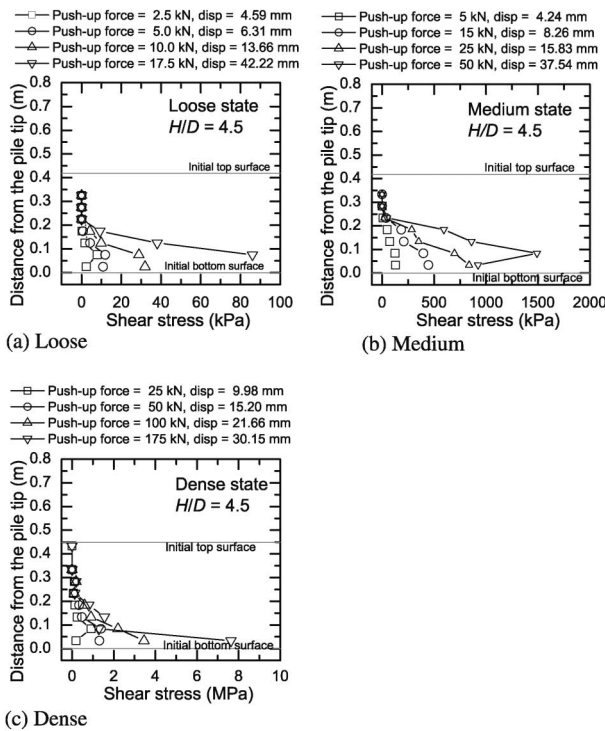


Fig. 13. Distribution of shear stress along model pipe pile where  $H/D = 4.5$

large difference in the push-up forces observed in the experiments by considering the changes in density alone. It is suggested that the dilatancy behaviour of the sand plug has a greater influence on the sand plug capacity than the density of the soil plug itself. This aspect will be discussed later through a comparison with theoretical values, the DEM analysis results and the experimental results.

Close inspection of the push-up load tests on the dense sand plug (Fig. 12(c)) indicates that there are two different shapes for the force-displacement relation. It is seen that there is a critical aspect ratio  $(H/D)_{crit}$ , which separates the two different shapes of that relation. When  $H/D$  was greater than  $(H/D)_{crit}$ , the push-up force developed rapidly with small push-up displacement and the relation had a concave curve. In contrast, when  $H/D$  was smaller than  $(H/D)_{crit}$ , the push-up force increased gradually when the push-up displacement increased and the relation had a convex curve.

Let us see here the results of the push-up load tests for the case of  $H/D = 4.5$  in detail. Figure 13 shows the distribution of mobilised shear stress acting along the inner pile shaft in the loose, the medium and the dense states. Shear stress levels were calculated from the measured axial forces down the pile. The results indicate that the shear stress increased exponentially from the top of the soil plug to the bottom, showing the well-known "silo effect". Very large shear stress was found in the area around the bottom of the sand plug. Hence, it is noted that the lower part of the sand plug, particularly the area adjacent to pile tip, mostly resists the push-up force. The other cases showed similar results to those of the push-up load tests for the case of  $H/D = 4.5$ .

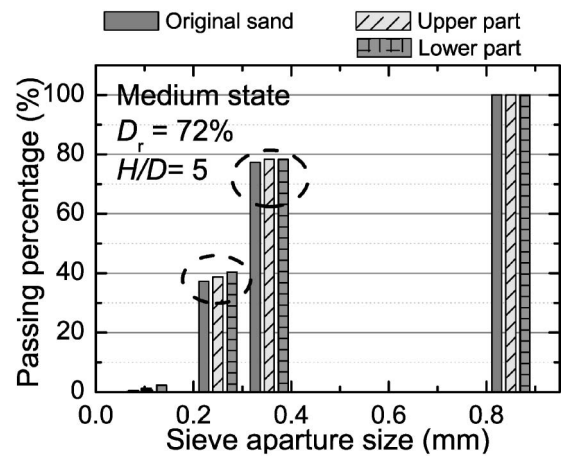


Fig. 14. Comparisons of sieve analysis results of upper and lower parts of sand plug after push-up load tests, together with grain size distribution of original sand

After completion of the push-up load test on the medium sand plug with  $H/D = 5$ , sieve analyses of the sand plug were carried out to investigate the occurrence of particle crushing, following the Standards of the Japanese Geotechnical Society for Laboratory Tests (1992). The sand plug was roughly divided into upper and lower portions. Sieve analyses were carried out separately for the upper and lower portions of the sand plug.

Figure 14 shows the sieve analysis results for the upper and lower portions of the sand plug compared with the original grain size distribution. The passing percentages of the silica sand finer than 0.4 mm, after the push-up load tests, were slightly higher than that of the original grain size. Close inspection of the sieve analyses shows that the sand from the lower portion of the soil plug had a larger amount of fines components than the upper portion of the soil plug, although the difference was very small. Moreover, particles finer than 0.2 mm were not found in the original sand, while they were detected after the push-up load tests. The results in Fig. 14 clearly show that the particle crushing of the silica sand occurs during the push-up loading.

In order to ensure the particle crushing phenomenon, oedometer tests on the loose, the medium and the dense sand specimens were carried out and sieve analyses of the soil specimens were conducted after the oedometer tests.

Figure 15 shows the results of the oedometer tests in terms of the effective vertical stress,  $p$ , versus the void ratio,  $e$ . The yield stress levels were estimated to be 2000 kPa, 1600 kPa and 1500 kPa for the loose, medium and dense specimens, respectively. It is seen that the compressibility of the loose specimen increased rapidly when  $p$  exceeded the yield stress, compared with the other specimens. The rate of increase in the compressibility of the medium specimen was higher than that of the dense specimen.

Figure 16 shows the results of the sieve analyses of the oedometer test specimens after effective vertical pressure,  $p$ , reached 4080 kPa. The results show that the passing

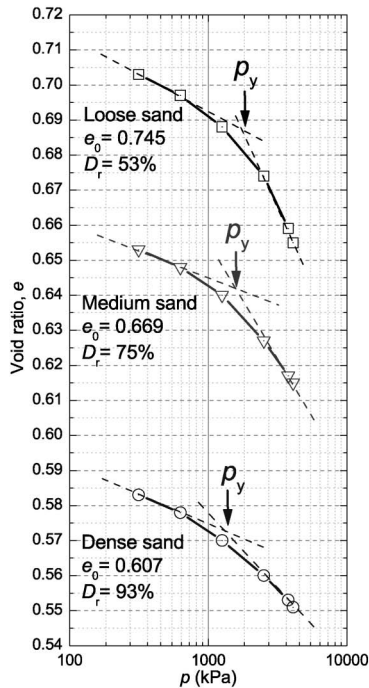


Fig. 15. Results of oedometer tests on loose, medium and dense sand specimens

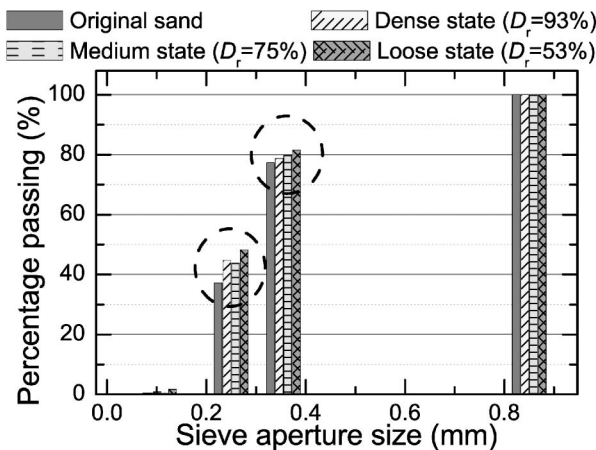


Fig. 16. Results of sieve analyses on specimens after oedometer tests

percentages of the silica sand particles finer than 0.4 mm, after the oedometer tests, are higher than the original grain size distribution, indicating that particle crushing occurred in all cases. A higher degree of particle crushing was observed in the loose specimen than in the medium or the dense specimens. Figures 15 and 16 indicate that a large amount of particle crushing would have occurred after  $p$  exceeded the yield stress.

In the push-up load tests on the sand plugs, the push-up force of 11.6 kN corresponded to the vertical stress of 1700 kPa at the bottom of the sand plug, which is the average yield stress of the loose, medium and dense specimens. This value is recognised as the threshold value where the particle crushing starts to occur. Therefore, particle crushing in the sand plug may have occurred in

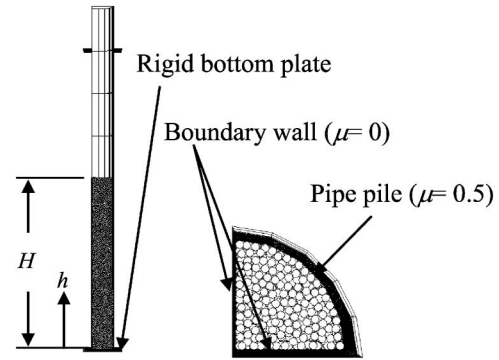


Fig. 17. Analysis model of push-up load tests of soil plug

several cases of push-up load tests, because the push-up forces exceed this threshold value.

### DEM Analyses of the Push-up Load Tests

#### (a) Simulation Procedure

DEM simulations of the push-up load tests on the silica sand plugs were carried out for the loose, medium and dense states without giving consideration to particle crushing. That is, the influence of particle crushing on the plugging behaviour was not taken into account in these DEM analyses. The analysis parameters listed in Table 4 were used for the numerical study on the push-up loading of sand plugs. The intrinsic friction coefficient between the clump and the wall was set at 0.5: it had been measured from the shear tests between the silica sand and the inner pile shaft. The aspect ratio of the soil plug height,  $H$ , to the inner diameter,  $D$ , was varied from 3 to 5, which corresponded to the experimental conditions.

Figure 17 shows the analysis model of push-up load tests on a soil plug. Considering the axi-symmetrical conditions of the problem, only one-fourth of the pile and the soil plug were modelled in order to reduce the calculation time. The pipe pile was modelled by rigid wall elements. Hence, the deformation of the pile was not taken into account in the analysis. The model pipe pile was 93.2 mm in inner diameter and 800 mm in length. The intrinsic friction coefficient between the model pile and the clump particles was set 0.5, which was obtained from the shear tests between the pile shaft and the sand particles (see Fig. 3), while the friction between the clumps and the boundary walls was assumed to be 0 (perfectly smooth).

In the DEM process, the clump particles were generated inside the model pile in order to form a soil plug without friction between the clump particles and the inner pile shaft. Then, a self-weight analysis was conducted. Finally, a simulation of the push-up loading was carried out by applying an upward velocity of 5 mm/s to the bottom plate and by taking the friction coefficient between the model pile and the clump particles into account.

Three series of simulations were carried out for the loose, medium and dense soil plugs. The number of clumps, the void ratio and the dry density of soil plug in each simulation are shown in Table 8.

**Table 8. Initial properties of soil plug in DEM analysis****a) Loose sand**

$H/D$	3.0	4.0	4.5	5.0
Number of clumps	5053	6768	7636	8500
Relative density, $D_r$ (%)	45	47	49	50
Void ratio, $e$	0.833	0.825	0.819	0.816
Dry density, $\rho_d$ ( $t/m^3$ )	1.491	1.498	1.502	1.505

**b) Medium sand**

$H/D$	3.0	4.0	4.5	5.0
Number of clumps	5227	7003	7906	8801
Relative density, $D_r$ (%)	66	69	71	72
Void ratio, $e$	0.772	0.763	0.758	0.754
Dry density, $\rho_d$ ( $t/m^3$ )	1.543	1.550	1.556	1.559

**c) Dense sand**

$H/D$	3.0	4.0	4.5	5.0
Number of clumps	5412	7253	8182	9100
Relative density, $D_r$ (%)	87	90	92	93
Void ratio, $e$	0.711	0.703	0.698	0.697
Dry density, $\rho_d$ ( $t/m^3$ )	1.597	1.605	1.610	1.611

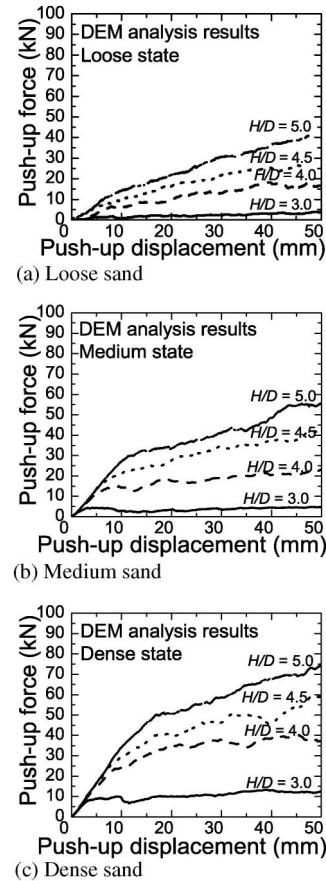
**(b) Simulation Results**

Figure 18 shows the relationship between the push-up displacement and the push-up force in each packing state. Note that the push-up force in Fig. 18 is four times the calculated value, because only one-fourth of the pile and the soil plug were modelled in the DEM analysis. The push-up force increases significantly with the increase in the  $H/D$  ratio or with the increase in the initial packing state of the soil plug. The push-up force in each case continued to increase with the increase in the push-up displacement. In the case of the dense state, only one form of the force-displacement relation (i.e., convex shape) was observed. This behaviour is in total contrast to the experimental results in which two forms (convex and concave shapes) for the relation were observed.

Let us see the results of the DEM simulations in detail. Figures 19, 20 and 21 show comparisons between DEM simulations and experimental results in the loose, medium and dense states, respectively.

According to the one-dimensional compression test results, the crushing of the soil particles starts to occur when the compression stress reaches a yield stress of about 1700 kPa, which corresponds to the threshold push-up force of 11.6 kN. The dashed lines in the figures indicate this threshold force. It is observed that DEM simulations show a good agreement with the experimental results in all the packing states as long as the push-up force does not exceed the threshold force.

Figure 22 shows a comparison of the distributions of inner shear stress obtained from the experiment and from the DEM analysis for the medium sand plug with  $H/D = 4.5$ . As mentioned earlier, the yield stress of the sand corresponds to the threshold push-up force,  $F$ , of 11.6 kN. Therefore, comparisons can be made for the cases where  $F$  is less than the threshold force (Fig. 22(a)) and where  $F$

**Fig. 18. Relationship between push-up displacement and push-up force in DEM**

is greater than the threshold force (Fig. 22(b)). Until the push-up force reached the threshold value, the DEM results showed a good agreement with the experimental results (Fig. 22(a)). On the contrary, after the push-up force exceeded the threshold force and increased, the DEM analyses tended to underestimate the inner shear stress levels, especially at the lower portion of the soil plug. Note here that a relatively large amount of particle crushing was observed in the experiments (see Figs. 14 and 16), although particle crushing was not modelled in the DEM analyses in this research. It should be emphasised again that the DEM simulated the experimental results well as long as the crushing of soil particles did not occur.

However, it is difficult to say that the crushing of soil particles during the push-up loading is the only significant factor influencing the discrepancy between the experimental results and the DEM results. Since the size of the clump used in the DEM is large, compared with the mean grain size of the silica sand, further laboratory tests and simulations are needed to establish the source of the discrepancy.

Figures 23, 24 and 25 show the changes in void ratio against the push-up displacement in the DEM analyses for the loose, medium and dense states, respectively. In order to calculate the void ratio of the soil plug during push-up loading, the soil plug was divided into several

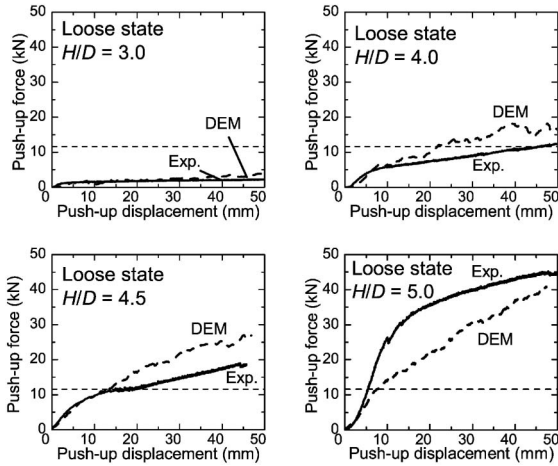


Fig. 19. Comparisons of push-up force and push-up displacement between DEM and the experiment (Loose packing state)

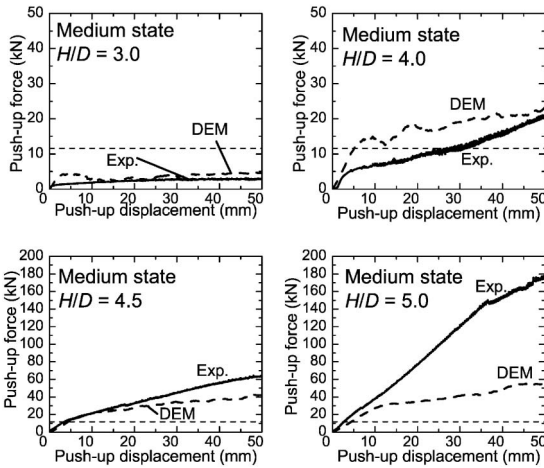


Fig. 20. Comparisons of push-up force and push-up displacement between DEM and the experiment (Medium packing state)

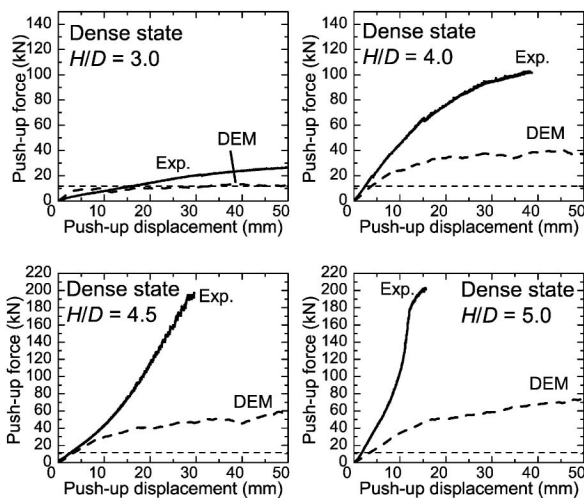
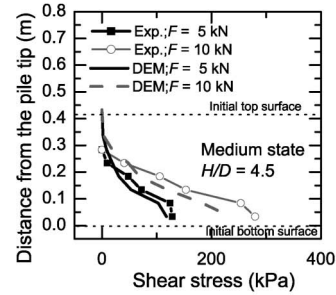
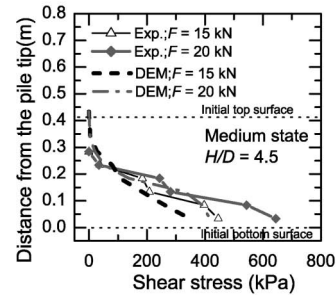


Fig. 21. Comparisons of push-up force and push-up displacement between DEM and the experiment (Dense packing state)



(a) For push-up force  $F$ , less than the threshold force



(b) After push-up force  $F$  exceeds the threshold force

Fig. 22. Comparisons of inner shear stress distributions obtained from the experiment and DEM analysis for medium packing state with  $H/D = 4.5$

zones denoted by the distance  $h$  measured from the bottom plate. The number of zones in each simulation depends on the  $H/D$  ratio of the soil plug. The results show that the void ratio in the lowest portion, adjacent to the bottom plate (Zone 1:  $h = 0$  to 100 mm), significantly decreases with the increase in the push-up displacement or the increase in the  $H/D$  ratio, except for the case of  $H/D = 3$ . Conversely, the void ratio in other zones changed slightly from the initial state and then showed a levelling off at a void ratio of 0.8, irrespective of the  $H/D$  ratio of the soil plug. So, it can be judged that the lower portion of the soil plug, adjacent to the pile tip, is gradually compressed and becomes denser with the increase in the push-up displacement and in  $H/D$ , except for  $H/D = 3$ . On the other hand, the density of the other portions of the plug changed a bit in the early loading stage and became constant.

Figure 26 shows the mobilised friction coefficient at the soil-pile interfaces in the DEM simulations for the dense state. The maximum mobilised friction coefficient was observed in the lower portion of the plug, corresponding to the maximum mobilised shear stress in that portion. This phenomenon proves that the lower part of the sand plug, adjacent to the pile tip, mostly resisted the push-up force.

According to the shear tests between the sand particle and the pile surface, the intrinsic sand-pile interface friction coefficient without particle rotation was 0.5, whereas the sand-pile interface friction with permission for sand particle rotation was 0.22. The results showed that the mobilised friction coefficient varied within the range of 0.22 to 0.5, indicating that the slipping and the rotation of the particles occurred simultaneously at the soil-pile

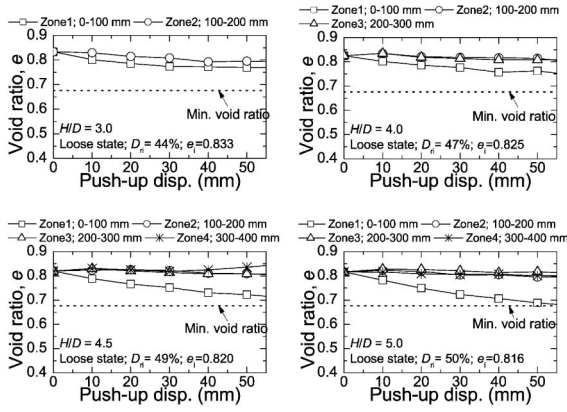


Fig. 23. Calculated distribution of void ratio during push-up loading (Loose state)

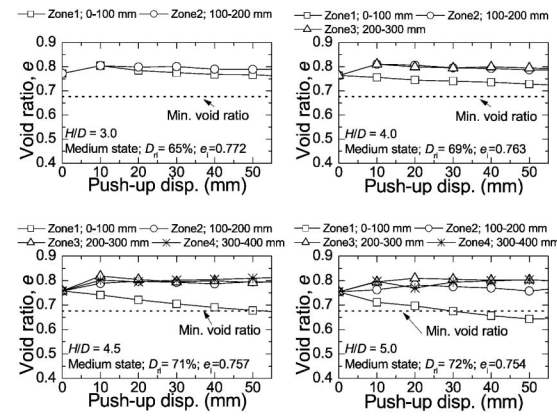


Fig. 24. Calculated distribution of void ratio during push-up loading (Medium state)

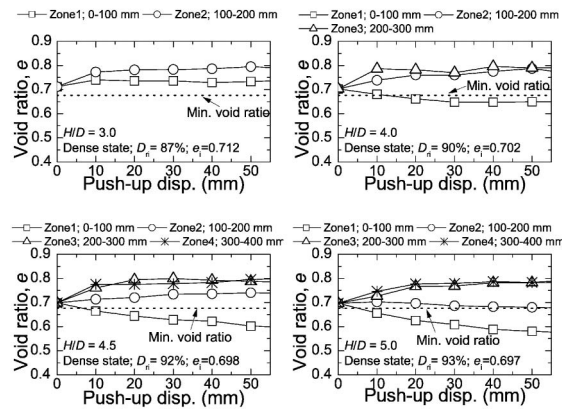


Fig. 25. Calculated distribution of void ratio during push-up loading (Dense state)

interface. It is also seen that the mobilised friction coefficient in the upper portion of the soil plug was smaller than that in the lower portion. This indicates that a larger degree of particle rotation occurs in the upper portion of the soil plug than in the lower portion.

The DEM results clearly show that the dilatancy behaviour in a soil plug is not uniform, but is dependent on the

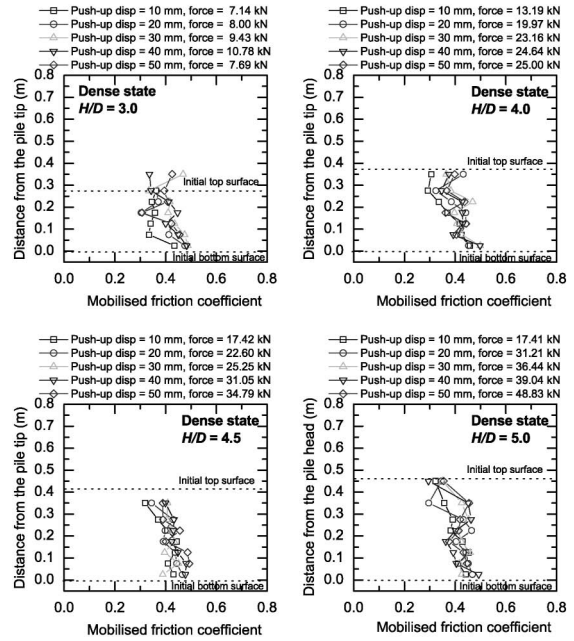


Fig. 26. Mobilised friction coefficient during push-up loading (Dense state)

location. These results are totally different from Yamahara’s assumption that soil plugs are modelled as rigid bodies.

### COMPARISON WITH YAMAHARA’S THEORETICAL EQUATION

Yamahara (1964a, b) proposed a theoretical Eq. (1) to give the maximum push-up force of a soil plug. According to this theory, the soil plug is assumed to be a rigid body, and Eq. (1) is derived from the equilibrium of forces acting on a thin soil plug element.

$$p(x) = \frac{\gamma' D}{4\mu K} \left( \exp\left(\frac{4\mu K}{D} x\right) - 1 \right) \quad (1)$$

where  $\gamma'$  is the effective unit weight of the soil,  $\mu$  is the coefficient of friction between the pile and the soil,  $K$  is the coefficient of the lateral pressure (ratio of lateral pressure to vertical pressure) and  $x$  is the distance from the top of the soil plug.

Table 9 shows the maximum push-up force in each  $H/D$  calculated by Yamahara’s equation. In the calculation, the value of  $K$  was estimated using the well-known Jaky’s equation, namely,

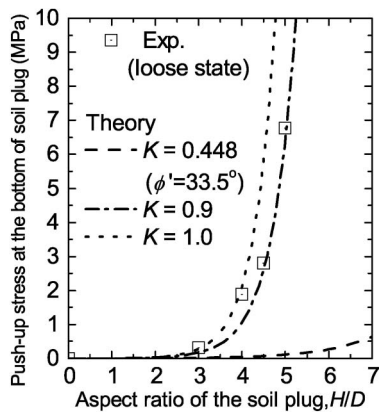
$$K = K_0 = 1 - \sin \phi' \quad (2)$$

A comparison of the results between Table 7, the experimental results, and Table 9, results of Yamahara’s equation, shows that the theoretical Eq. (1) underestimates the maximum push-up force observed in the experiments to an excessive degree.

Figure 27 shows the relationships between the  $H/D$  ratio and the maximum push-up stress at the bottom of the soil plug obtained from Eq. (1) and measured from the experiments for the loose sand case. The  $K$ -value in the

**Table 9.** Calculated value of maximum push-up force by Yamahara's equation

$H/D$	Maximum push-up force (kN)		
	Loose	Medium	Dense
3.0	0.15	0.14	0.14
4.0	0.37	0.33	0.33
4.5	0.59	0.51	0.50
5.0	0.93	0.78	0.76
6.0	2.29	1.84	1.75

**Fig. 27.** Comparison of maximum push-up stress from Yamahara's theory and experiments for loose sand plug

calculation was back-figured in order to fit the experimental results for each  $H/D$ . In other words, if the value of the internal friction angle,  $\phi' = 33.5^\circ$ , obtained from the direct shear tests was used, the experimental results were not able to be predicted by Eq. (1). It is also seen that it is difficult to fit the experimental results for various  $H/D$  by employing a single value of  $K$ . The value of  $K$  which simulates the experimental results ranges from 0.9 to 1.0. Similar results were obtained for both medium and dense soil plug cases.

It should be noted that influence of the dilatancy behaviour of the soil plug is not taken into account in Yamahara's theory. Hence, the large discrepancy between the experiments and the calculated values seems to be caused by the influence of the dilatancy behaviour of the soil plugs. In addition, high  $K$ -values suggest particle crushing in the soil plug, because  $\phi'$  tends to decrease with the increase in particle crushing, cf. Eq. (2).

## CONCLUSIONS

The main objective of this paper was to investigate the plugging mechanism and the formation of soil plugs during the push-up loading of the soil plugs using experimental and numerical studies. Focus was placed on the influence of the packing state (relative density) and the  $H/D$  ratio of the soil plugs. The main conclusions are as follows:

In the experimental study, push-up load tests on the silica sand plugs were carried out. It was observed that the

push-up force increases significantly with the increase in the  $H/D$  ratio and the packing state of the soil plugs.

Considering close inspection in the case of a dense sand plug, there is a critical aspect ratio,  $(H/D)_{crit}$ , which separates the two different shapes of the load-displacement relation. When  $H/D$  is greater than  $(H/D)_{crit}$ , the push-up force develops rapidly with small push-up displacement having a concave shape. In contrast, when  $H/D$  is smaller than  $(H/D)_{crit}$ , the push-up force increases gradually with the increase in push-up displacement having a convex shape.

The experimental results also show that maximum mobilised shear stress was observed in the lower portion of the soil plug in all cases, indicating that the lower portion of the soil plug plays an important role in the push-up force.

Based on the sieve analysis results, the crushing of soil particles occurs during the push-up loading especially for the lower portion of the soil plugs.

In the numerical study, although the DEM simulations of the push-up load tests were carried out under unrealistic conditions, using a larger particle size than the real size, the DEM results show a reasonable agreement with the experimental results as long as soil particle crushing does not occur. The DEM was also able to estimate the influence of the  $H/D$  ratio and the packing state on the soil plug capacity.

Based on the calculated distribution of void ratios, it can be judged that the lower portion of the soil plug, adjacent to the pile tip, is compressed gradually and becomes denser with the increase in push-up displacement as well as the increase in  $H/D$ . In contrast, the density of the other portions of the plug changes a bit in the early state and then becomes constant. The results indicate that the dilatancy behaviour in soil plugs is not uniform, but is dependent on the location of the soil plug.

Furthermore, the mobilised friction coefficient showed that the rotation of sand particles occurs in the vicinity of the soil-pile interface and seems to be a parameter of influence on the soil plug capacity.

In comparison with the theoretical equation derived by Yamahara, the experimental results for various  $H/D$  cannot be evaluated by Yamahara's equation employing a constant  $K$ -value. It should be noted that the influence of the dilatancy behaviour of the soil plug is not taken into account in Yamahara's equation.

Although this study has been carried out under ideal conditions, the experimental and DEM simulation results reveal such interesting issues as particle crushing and particle rotation during push-up loading. Further numerical studies, using a small particle size, will help to deepen the understanding of the plugging mechanism.

## REFERENCES

- 1) Byrne, B. W. (1995): Driven pipe piles in dense sand, *Australian Geomechanics*, 27, Paper No. 9501, 72-80.
- 2) de Nicola, A. and Randolph, M. F. (1997): The plugging behaviour

- of driven and jacked piles in sand, *Géotechnique*, **47**(4), 841–856.
- 3) Cundall, P. A. and Strack, O. D. L. (1979): Discrete numerical model for granular assemblies, *Géotechnique*, **29**(1), 47–65.
  - 4) Gavin, K. G. and Lehane, B. M. (2003): The shaft capacity of pipe piles in sand, *Canadian Geotechnical Journal*, **40**(1), 36–45.
  - 5) Hight, D. W., Lawrence, D. M., Farquhar, G. B., Milligan, G. W. E., Gue, S. S. and Potts, D. M. (1996): Evidence for scale effects in the end bearing capacity of open-ended piles in sand, *Proceedings of 28th Offshore Technology Conference*, Texas, 181–192.
  - 6) Härtl, J. and Ooi, J. (2008): Experiments and simulations of direct shear tests: porosity, contact friction and bulk friction, *Granular Matter*, **10**(4), 263–271.
  - 7) Itasca (2003): PFC3D Manual, Itasca Consulting Group, USA.
  - 8) Japanese Geotechnical Society (1992): Standards of Japanese Geotechnical Society for Laboratory Test (in Japanese).
  - 9) Kanno, T., Yamakawa, S., Onishi, M. and Miura, H. (1978): Blockade sand effect of large diameter open-ended pipe piles, *Technical report of Sumitomo Metal Industries*, **30**(1), 52–61 (in Japanese).
  - 10) Katzenbach, R. and Schmitt, A. (2004): Micromechanical modeling of granular materials under triaxial and oedometric loading, *Proceedings of 2nd International PFC Symposium*, Kyoto, 313–322.
  - 11) Kishida, H. and Isemoto, N. (1977): Behaviour of sand plugs in open-ended steel pipe piles, *Proceedings of 9th International Conference on Soil Mechanics*, Tokyo, 1, 601–604.
  - 12) Kitiyodom, P., Matsumoto, T., Hayashi, M., Kawabata, N., Hashimoto, O., Ohtsuki, M. and Noji, M. (2004): Experiment on soil plugging of driven open-ended steel pipe piles in sand and its analysis, *Proceedings of 7th International Conference on the Application of Stress-Wave Theory to Piles*, Selangor, 447–458.
  - 13) Leong, E. C. and Randolph, M. F. (1991): Finite element analyses of soil plug response, *International Journal for Numerical and Analytical Methods in Geomechanics*, **15**, 121–141.
  - 14) Liyanapathirana, D. S., Deeks, A. J. and Randolph, M. F. (1998): Numerical analysis of soil plug behaviour inside open-ended piles during driving, *International Journal for Numerical and Analytical Methods in Geomechanics*, **22**, 303–322.
  - 15) Lianapathirana, D. S., Deeks, A. J. and Randolph, M. F. (2000): Numerical modelling of large deformations associated with driving of open-ended piles. *International Journal for Numerical and Analytical Methods in Geomechanics*, **24**, 1079–1101.
  - 16) Liyanapathirana, D. S., Deeks, A. J. and Randolph, M. F. (2001): Numerical modelling of the driving response of thin-walled open-ended piles, *International Journal for Numerical and Analytical Methods in Geomechanics*, **25**, 933–953.
  - 17) Matsumoto, T. and Takei, M. (1991): Effect of soil plug on behaviour of driven pipe pile, *Soil and Foundation*, **31**(2), 14–34.
  - 18) Matsumoto, T., Kitiyodom, P., Wakisaka, T. and Nishimura, S. (2004): Research on plugging of open-ended steel pipe piles and practice in Japan, *Proceedings of 7th International Conference on the Application of Stress-Wave Theory to Piles*, Selangor, 133–152.
  - 19) O'Sullivan, C., Cui, L. and Bray, J. D. (2004): Three-dimensional discrete element simulations of direct shear tests, *Proceedings of 2nd International PFC Symposium*, Kyoto, 373–382.
  - 20) Ovesen, N. K. (1979): The scaling law relationship—Panel Discussion, *Proceedings of the 7th European Conference on Soil Mechanics and Foundation Engineering*, **4**, 319–323.
  - 21) Paik, K. H. and Salgado, R. (2003): Determination of bearing capacity of open-ended piles in sand, *Journal for Geotechnical and Geoenvironmental Engineering*, ASCE, **129**(1), 46–57.
  - 22) Paik, K. H., Salgado, R., Lee, J. H. and Kim, B. J. (2003): The behaviour of open- and closed-ended piles driven into sands, *Journal for Geotechnical and Geoenvironmental Engineering*, ASCE, **129**(4), 296–306.
  - 23) Paikowsky, S. G. and Whitman, R. V. (1990): The effects of plugging on pile performance and design, *Canadian Geotechnical Journal*, **27**, 429–440.
  - 24) Randolph, M. F., Leong, E. C. and Houlsby, G. T. (1991): One-dimensional analysis of soil plugs in pipe piles, *Geotechnique*, **41**(4), 587–598.
  - 25) Randolph, M. F., May, M., Leong, E. C., Hyden, A. M. and Murff, J. D. (1992): Soil plug response in open-ended pipe piles, *Journal of Geotechnical Engineering*, ASCE, **118**(5): 743–759.
  - 26) Thongmune, S., Kobayashi, S. and Matsumoto, T. (2010): DEM simulations of push-up load tests of sand plug in steel pipe pile. *Int. Sym. on Geomechanics and Geotechnics: From Micro to Macro (IS-Shanghai 2010)*, Shanghai, 721–726.
  - 27) Yamahara, H. (1964a): Plugging effects and bearing mechanism of steel pipe piles, *Transaction of the Architectural Institute of Japan*, **96**, 28–35 (in Japanese).
  - 28) Yamahara, H. (1964b): Plugging effects and bearing mechanism of steel pipe piles (Part 2), *Transaction of the Architectural Institute of Japan*, **97**, 34–41 (in Japanese).
  - 29) Yan, W. M. (2009): Fabric evolution in a numerical direct shear test, *Computers and Geotechnics*, **36** (4), 597–603.